# Nanotechnology Reviews ‘Just Accepted’ Papers

**Nanotechnology Reviews (Nanotechnol Rev) ‘Just Accepted’ Papers** are papers published online, in advance of appearing in the layouted final online and print versions of the journal. The papers have been peer-reviewed and/or approved for publication by the Editors and are online published in manuscript form, but have not been copy edited, typeset, or proofread. Copy editing may lead to small differences between the Just Accepted version and the final version. There may also be differences in the quality of the graphics. When papers do appear in print, they will be removed from this feature and grouped with other papers in an issue.

**Nanotechnol Rev ‘Just Accepted’ Papers** are citable; the online publication date is indicated on the Table of Contents page, and the article’s Digital Object Identifier (DOI), a unique identifier for intellectual property in the digital environment (e.g., 10.1515/NTREV-2011-xxxx), is shown at the top margin of the title page. Once an article is published as **Nanotechnol Rev ‘Just Accepted’ Paper** (and before it is published in its final form), it should be cited in other articles by indicating author list, title and DOI.

After a paper is published in **Nanotechnol Rev ‘Just Accepted’ Paper** form, it proceeds through the normal production process, which includes copy editing, typesetting and proofreading. The edited paper is then published in its final form in a regular print and online issue of **Nanotechnol Rev.** At this time, the **Nanotechnol Rev ‘Just Accepted’ Paper** version is replaced on the journal Web site by the final version of the paper with the same DOI as the **Nanotechnol Rev ‘Just Accepted’ Paper version.**

**Disclaimer**

**Nanotechnol Rev ‘Just Accepted’ Papers** have undergone the complete peer-review/approval for publication process. However, none of the additional editorial preparation, which includes copy editing, typesetting and proofreading, has been performed. Therefore, there may be errors in articles published as **Nanotechnol Rev ‘Just Accepted’ Papers** that will be corrected in the final print and online versions of the Journal. Any use of these articles is subject to the explicit understanding that the papers have not yet gone through the full quality control process prior to advanced publication.

Brought to you by | University of Sussex Library
Authenticated
Download Date | 9/26/17 8:16 AM

*Nanotechnology Reviews* **'Just Accepted' paper**
**ISSN (online) 2191-9097**
**DOI: 10.1515/ntrev-2017-0165**

**Regulatory Issues in Nanotechnology contribution**

# Carbohydrate–protein interactions characterized by Dual polarization hybrid plasmonic waveguide

Chen Chen, Xun Hou and Jinhai Si,*

Key Laboratory for Physical Electronics and Devices of the Ministry of Education and Shaanxi Key Lab of Information Photonic Technique, School of Electronics and Information Engineering, Xi'an Jiaotong University, Xi'an 710049, China

*Corresponding author

e-mail: *jinhaisi@mail.xjtu.edu.cn



Brought to you by | University of Sussex Library
Authenticated
Download Date | 9/26/17 8:16 AM

## Abstract

Optical biosensors present good performance for affinity analysis of molecular binding event. However, most of those excited with single optical mode are “blind” to the conformational change of bound molecules. We theoretically demonstrate a dual polarization hybrid plasmonic (DPHP) waveguide with nano-slots. By addressing the structure with dual polarizations, the optogeometrical properties (density and thickness) of protein layers have been determined without ambiguity. Differences in the hybrid mode dispersion between the transverse electric (TE) and transverse magnetic (TM) modes allow separately determine the thickness and the density at all stages during the molecular interaction. In addition, Nano-slots can be equated with an effective optical capacitance resulting in strong field confinement, thereby subtle changes in the ambient medium can be sensed. A proof of concept is conducted by analyzing the conformational change of HepV, a recombinant fragment of collagen V, during complicated molecular interaction. Integrated with adlayer thickness and density, we can conclude that a thick sparse layer formed after heparin capture and a thin dense layer arising from HepV bound. Accordingly, HepV undergoing conformational change has been traced and verified as molecular interaction occurs.


**Keywords:** dual polarization, hybrid plasmonic, waveguide, conformational change, biosensing



Brought to you by | University of Sussex Library
Authenticated
Download Date | 9/26/17 8:16 AM

# 1. Introduction

Biomolecules exert their biological effects via binding to other molecules. A significant number of interactions including antibody–antigen[1], receptor–hormone[2] and enzyme–substrate[3] play a crucial role in physiological activities. Thus, precise detection of biomolecules especially proteins is strongly required in the medical and bioprocess[4,5]. Nuclear Magnetic Resonance (NMR) with isotope-labeled biological sample is common used for determining protein conformation, yet high-quality protein consumption[6]. Without sacrificing the resources for more extensive biophysical characterization, label-free biochemical technologies, particularly evanescent wave biosensor techniques[7]-[12] such as surface plasmon resonance (SPR)[13]-[15], provide considerable insight into biological events. The physics of SPR techniques relies on measurements to single transverse magnetic (TM) polarization[16]. Due to single measurement, it is unable to differentiate shifts in the biolayer thickness $\Delta a$ and refractive index $\Delta n_l$. Thus, SPR is hardly capable of distinguishing between a thick sparse layer and a thin dense layer. This means such technology is "blind" to the conformational change of bound molecules. To gain greater information of biological events taking place at these interfaces two measurements are required. Moreover, researchers lay increasing stress on the concept of proteome which can be broadly interpreted as proteins expressed by genome, resulting in an obvious requirement for huge collaborative effort in protein signature[17]. Given that TE and TM modes excited simultaneously, both $\Delta a$ and $\Delta n_l$ can be traced without ambiguity. Recently, a dual polarization interferometry (DPI)[18,19] with its ability to monitor conformational change of molecules has been deployed in the field of protein engineering. This commercially available approach has been demonstrated to provide both adlayer thickness $a$ and refractive index $nl$ in the biological system such as protein-protein interaction. However, this technique lacks multiplexing abilities and suffers from a large footprint, setting limits on the development and application as biosensor[20].

In this work, we investigate a dual polarization hybrid plasmonic (DPHP) waveguide. Two orthogonal polarizations of incident light are applied to the chip, in turn exciting the fundamental quasi-TE mode and fundamental quasi-TM mode (hereafter this text will be abbreviated as TE mode and TM mode) and the modes interrogate the biolayer by means of evanescent tail[21,22]. In this way, shifts in adlayer thickness $\Delta a$ and refractive index $\Delta n_l$ can be determined independently. Moreover, nano-slots formed between a metal (Ag) cladding and a silicon core can provide a combination of plasmonic and photonic modes contributing



Brought to you by | University of Sussex Library
Authenticated
Download Date | 9/26/17 8:16 AM

to sub-wavelength confinement with high sensitivity as well as relative long propagation distance. We adopt resonance wavelength shift to interpret the molecular event. In order to verify the novel architecture, we quantitatively analyze the carbohydrate-protein interaction in which biotinylated heparin is immobilized to the surface through biotin–streptavidin system subsequently, interacting with HepV, a recombinant fragment of collagen V. Collagen V[23,24] is a member of the fibril subclass of collagens and it plays crucial role in fibrillogenesis[23,24]. This collagen controls the initiation of collagen fibril assembly and acts as an adhesive substrate for a large variety of cells. Collagen V specifically interacts with a number of extracellular components through its 300nm long predominant triple helical domain which exhibits different molecular forms in tissue[24]. The major form in most tissues is the heterotrimer [α1(V)]2α2(V) which was previously discovered to interact with heparin depending on glycosaminoglycans chains at physiological salt concentrations[24]. Specifically, the heparin binding region is located within a 12kDa fragment in the triple helical part of the a1(V) chain[24,25]. The recombinant fragment (Ile824 to Pro950), referred as HepV, is sufficient for heparin binding and functions as cell adhesion through a cell surface heparan sulfate proteoglycan[24,25]. Therefore, the binding of HepV to heparin can modulates the interaction between collagen V and heparin sulfate proteoglycan in tissues. D-biotin streptavidin model which has been intensely investigated for decades and is used in immunological protocol is utilized for immobilizing heparin on the surface owing to its high binding affinity with dissociation constant of $K_d$=$10^{-15}$ mol/$dm^3$[26]. The whole process of HepV-heparin interaction is simulated based on finite-element-method (FEM) via the commercially available software, COMSOL Multiphysics with success.

# 2. Design of DPHP waveguide

## 2.1 Schematic of DPHP waveguide

Figure 1a presents the 3D schematic structure of proposed DPHP waveguide, consisting of a silicon-on-insulator(SOI) rib and a metal (Ag) cladding. The region between Si core and Ag layer is filled with tested analyte. In this way, double nano-slots are formed at both sides of the Si core as well as another slot embedded on the top of Si core. The cross-section view with geometric parameters is presented in Fig.1b. The widths of Si core and lateral nano-slot are denoted as $w_{si}$ and $w_{slot}$, respectively. The height of Si ridge and upper nano-slot are defined as $h_{si}$ and $h_{slot,}$ respectively. The optimized values of $w_{slot}$ and $h_{slot}$ are setting as 40nm



Brought to you by | University of Sussex Library
Authenticated
Download Date | 9/26/17 8:16 AM

and 60nm respectively, giving rise to strong filed confinement and low propagation loss. In Fig.1c, field profile obtained by simulation, reveals that present configuration can support both TE and TM modes. Assign the values of geometric parameters: $w_{si}$ equals 550nm; $h_{si}$ equals 320nm; $h_{sio2}$ (substrate) is 3μm high and the length of waveguide ($l$) is 25μm. The thickness of Ag cladding are setting as 3μm so as to neglect the influence of simulation boundaries. This structure is manipulated compatibly with conventional SOI optical as well. In the simulation work, the refractive indices[27] of Si and $SiO_2$ are set as 3.5046 and 1.447, respectively, at central wavelength of 1.3μm. The wavelength selection[7] is based on a tradeoff between the absorption loss caused by aqueous solution and the broadband light sources. Water solution optical absorption is smaller at wavelength of 1.3μm, compared with 1.55μm wavelength common used for operation. The permittivity of silver is achieved through Durde model[28]:

$$\varepsilon = \varepsilon_{\infty} - \frac{\omega_{\mathrm{p}}^2}{\omega^2 + j\omega\gamma} \tag{1}$$

with $\varepsilon_{\infty} = 3.1$, $\omega_p = 140\times10^{14} rad/s$, and $\gamma = 0.31\times10^{14}\ rad/s$.

## 2.2 Theory of DPHP waveguide

For most waveguide systems, the evanescent wave decays exponentially with decay length on the order of 0.1-1μm[20], thus it only senses the changes taking place on the surface of waveguide due to higher intensity of evanescent field in this particular region. Therefore, the shifts in bulk solution is hardly considered, whereas the bulk index has exact influence on the sensor response. With regard to the proposed structure, incident light goes through the waveguide and excites surface plasmon in the slots when the phase velocities of the optical mode and that of the surface plasmon match. The field is highly confined in the slots and sufficiently penetrates into solution. As a result the bulk refractive index can be measured. Evidently, the slots are able to store electromagnetic energy resulting in subwavelength optical guiding with lower propagation loss. Since the dielectric discontinuity at Si core-solution interface produces a polarization charge[29] which interacts with the plasma oscillations of the metal–solution interface. The gap region can be equated with an effective optical capacitance[29] resulting in strong field confinement and lower propagation loss. Propagation constant of surface plasmon depends strongly on the wavelength, in comparison with optical modes of traditional dielectric waveguide. Phase-matching condition between an



Brought to you by | University of Sussex Library
Authenticated
Download Date | 9/26/17 8:16 AM

optical mode of dielectric waveguide and a surface plasmon supported by metal (Ag) cladding might be fulfilled within a narrow spectral band. Therefore, when a broadband light (1.285μm ≤ λ ≤ 1.315μm in this case) is applied to the waveguide, the spectrum presents a narrow dip with optical energy conversion into surface plasmon[35]. The position of resonance dip in the output spectrum strongly relies on the refractive index of sensed medium. Any changes of the sensed medium will alter the resonance condition which results in a shift of the resonance dip. Thus, we can adopt wavelength interrogation to interpret the molecular interaction.

## 2.3 Carbohydrate–protein interactions based on DPHP waveguide

Herein, HepV-heparin interaction was emulated based on finite-element-method (FEM) and carried out with COMSOL. Generally, HepV-heparin binding event can be simplified to four distinct steps[25]: (1) Tris buffer flowing over the biotin functionalized waveguide surface for initial calibration, (2) streptavidin immobilized on the surface, (3) capture of biotinylated heparin, (4) introducing recombinant HepV fragment to recognize biotinylated heparin. During the biological event, thickness $a$ and refractive index $n_l$ of adlayer with known numerical value were obtained from typical literature data[25]. Besides, bulk refractive indices in this case were calculated according to empirical equation[25] expressed as $n_l$=0.52*($n_p$ – $n_s$) + $n_s$, where $n_p$ is the refractive index of pure protein (1.465)[31]-[33] or solvated carbohydrate (1.45)[34]. All data including $n_l$, $n_s$ and $a$ are presented in the table 1. The effective mode indices ($n_{eff\_TE}$ and $n_{eff\_TM}$) were measured for wavelength spanning 1.285μm≤$\lambda$≤1.315μm at all stages. The fitting curves of the $n_{eff\_TE}$ and $n_{eff\_TM}$ *versus* the wavelength $\lambda$ are plotted in Fig.2. One can see clearly the process of HepV-heparin binding event in the whole spectrum range. Shifts of resonance wavelength depending on the effective mode indices of the waveguide are significant different. Thus, we can take wavelength interrogation to interpret the molecular interaction.

## 2.4 Property of DPHP waveguide

In general, sensitivity and propagation loss are considered as a significant criteria to evaluate the performance of biosensor. It is necessary to validate these two physical quantities of the proposed DPHP waveguide. The waveguide sensor sensitivities respond to (1) the changes of bulk refractive index $\Delta n_s$, (2) the shifts in biolayer index $\Delta n_l$ and (3) adlayer thickness variation $\Delta a$. In the molecular interaction, all the effects occur and consequently, the resulting effective mode index change is



Brought to you by | University of Sussex Library
Authenticated
Download Date | 9/26/17 8:16 AM

$$\Delta n_{eff\_i} = \frac{\partial n_{eff\_i}}{\partial n_s}\Delta n_s + \frac{\partial n_{eff\_i}}{\partial n_l}\Delta n_l + \frac{\partial n_{eff\_i}}{\partial a}\Delta a \ (i=TE,TM) \quad (2)$$

where $\frac{\partial n_{eff\_i}}{\partial n_s}$ , $\frac{\partial n_{eff\_i}}{\partial n_l}$ and $\frac{\partial n_{eff\_i}}{\partial a}$ represent respectively the shifts in bulk index, in biolayer index and thickness contributing to the effective mode indices. For wavelength shift detection, we investigate transmission spectrum on resonance wavelength spanning 1.285μm≤λ≤ 1.315μm. The data were plotted in Fig.3. The position resonance dip dependent on the effective mode index of waveguide as well as polarization. With the process of molecular event, the resonance wavelength for TE mode moves to short-wave direction, while for TM mode, resonance wavelength shifts toward longer wavelength. Various numerical values of blue-shifted and red-shifted wavelengths arise from different influence of effective mode index, which are also in agreement with the results in Fig.2. For TE mode, compared with Tris buffer calibration, resonance wavelength caused by streptavidin immobilization is blue shifted 6nm, while resonance wavelengths induced by heparin capture and HepV binding are blue shifted 2nm and 4nm respectively. For TM mode, a redshift of 8nm with streptavidin immobilization and that of 12.5nm and 10nm with heparin capture and HepV binding respectively are presented.

Afterwards, the spectral interrogation sensitivities, caused by changes of bulk refractive index $\Delta n_s$ for dual polarizations can be defined as follow:

$$S_{DPHP\_ns\_i} = \frac{\partial \lambda}{\partial n_s} = \frac{\partial \lambda}{\partial n_{eff\_i}} \cdot \frac{\partial n_{eff\_i}}{\partial n_s} \ (i=TE,TM) \quad (3)$$

where $\frac{\partial \lambda}{\partial n_{eff\_i}}$ is resonance wavelength shift caused by effective mode index of DPHP waveguide which were measured at each step (Fig.2), and $\frac{\partial n_{eff\_i}}{\partial n_s}$ represents the effects of buffer solution on effective mode index. Similarly, the spectral interrogation sensitivities, due to adlayer index variation $\Delta n_l$ can be interpreted as below:

$$S_{DPHP\_nl\_i} = \frac{\partial \lambda}{\partial n_l} = \frac{\partial \lambda}{\partial n_{eff\_i}} \cdot \frac{\partial n_{eff\_i}}{\partial n_l} \ (i=TE,TM) \quad (4)$$

where $\frac{\partial n_{eff\_i}}{\partial n_l}$ is the change of effective mode index resulted from adlayer indices. Apart from $\Delta n_s$ and $\Delta n_l$, the spectral interrogation sensitivities caused by adlayer thickness can be expressed:

$$S_{DPHP\_a\_i} = \frac{\partial \lambda}{\partial a} = \frac{\partial \lambda}{\partial n_{eff\_i}} \cdot \frac{\partial n_{eff\_i}}{\partial a} \ (i=TE,TM) \quad (5)$$



Brought to you by | University of Sussex Library
Authenticated
Download Date | 9/26/17 8:16 AM

where $\frac{\partial n_{eff\_i}}{\partial a}$ represents shift in adlayer thickness contributing to effective mode index of waveguide. Therefore, the resonant wavelength shift in complete formula is:

$$\Delta\lambda_{DPHP\_i} = S_{DPHP\_ns\_i}\,\Delta n_s + S_{DPHP\_nl\_i}\,\Delta n_l + S_{DPHP\_a\_i}\,\Delta a \ (i=TE,TM) \quad (6)$$

where $\Delta\lambda_{DPHP\_i}$ is the shift of resonance wavelength and $\Delta n_s$, $\Delta n_l$ and $\Delta a$ are shifts in bulk index, adlayer index and thickness in each step (excluding step 1) compared with calibration step.

In order to investigate propagation loss for hybrid plasmonic waveguide, optical confinement factor Γ defined previously[36] which was power confined in particular area divided the total power was introduced. It has been shown[36] that Γ is not only influenced by loss-less photonics mode but also by lossy plasmonic mode. Thus, we can improve $\Gamma_{layer}$ (power confined in layer compared with total power) by tuning the geometrical properties of structure to gain lower loss. The optimized size of waveguide is setting as aforementioned: $w_{slot}$=40nm, $h_{slot}$=60nm, $w_{si}$=550nm, $h_{si}$=320nm, $h_{Ag}$=3μm, $h_{sio2}$=3μm and $l$=25μm. To calculate the propagation loss, we derive loss coefficient α (in $dB/\mu m$) as the following equation: $\alpha = -1g\frac{P_o}{P_i}/2\lg e$ with Po power outflow time average (w) and Pi power inflow time average (w) and depict loss variation at wavelength spanning 1.285μm≤$\lambda$≤1.315μm in Fig.4. The propagation loss was measured for optimized dimension of DPHP waveguide with water solution for simplicity. It is presented that the optimum value for propagation loss achieves as low as the order of $10^{-4}$.

## 2.5 Characterization of heparin-Hep V interaction

To extract biolayer thickness and index, we rewrite equation6 with fixed wavelengths at resonance dips (λ=1.291μm, λ=1.295μm, λ=1.293μm for TE mode and λ=1.303μm, λ=1.3075μm, λ=1.305μm for TM mode):

$$\begin{bmatrix}\Delta\lambda_{DPHP\_TE}\\ \Delta\lambda_{DPHP\_TM}\end{bmatrix} = \begin{bmatrix}\frac{\partial\lambda_{TE}}{\partial n_s} & \frac{\partial\lambda_{TE}}{\partial n_l} & \frac{\partial\lambda_{TE}}{\partial a}\\ \frac{\partial\lambda_{TM}}{\partial n_s} & \frac{\partial\lambda_{TM}}{\partial n_l} & \frac{\partial\lambda_{TM}}{\partial a}\end{bmatrix}\cdot\begin{bmatrix}\Delta n_s\\ \Delta n_l\\ \Delta a\end{bmatrix} \quad (7)$$

where $\Delta\lambda_{DPHP\_i}$ ($i$=$TE,TM$) are shifts of resonance wavelength at all stages compared with Tris buffer calibration and the numerical values can be achieved via Fig.3. $\frac{\partial\lambda_i}{\partial n_s}$, $\frac{\partial\lambda_i}{\partial n_l}$ and $\frac{\partial\lambda_i}{\partial a}$ ($i$=$TE,TM$) are wavelength shifts induced by bulk index, adlayer index and thickness



Brought to you by | University of Sussex Library
Authenticated
Download Date | 9/26/17 8:16 AM

respectively. To calculate $\frac{\partial \lambda_{-}}{\partial n_{s}}$ for example, we can divide the term into $\frac{\partial \lambda}{\partial n_{eff,i}}$ which can be obtained through Fig. 2 and $\frac{\partial n_{eff,i}}{\partial n_{s}}$ which can be measured at resonance dips at each step(Fig.5) and subsequently do the math. With the same method, $\frac{\partial \lambda_{-}}{\partial n_{l}}$ and $\frac{\partial \lambda_{-}}{\partial a}$ can be achieved when integrated with Fig.2 and Fig.6 and Fig.7. For the relationship between bulk index and adlayer index in this case, $n_l$=0.52*($n_p$ – $n_s$) + $n_s$, the expression simplifies to:

$$\begin{bmatrix} \delta\lambda_{DPHP\_TE} \\ \delta\lambda_{DPHP\_TM} \end{bmatrix} = \begin{bmatrix} \frac{\partial \lambda_{-}TE^{*}}{\partial n_{l}} & \frac{\partial \lambda_{-}TE}{\partial a} \\ \frac{\partial \lambda_{-}TM^{*}}{\partial n_{l}} & \frac{\partial \lambda_{-}TM}{\partial a} \end{bmatrix} \cdot \begin{bmatrix} \delta n_{l} \\ \delta a \end{bmatrix} \tag{8}$$

It is noteworthy that to simplify the numerical calculation, we substitute $n_s$ with $n_l$ via empirical formula[25] $n_l$=0.52*($n_p$ – $n_s$) + $n_s$, and thus combine $\frac{\partial \lambda_{-}TE}{\partial n_{s}}$ with $\frac{\partial \lambda_{-}TE}{\partial n_{l}}$, and $\frac{\partial \lambda_{-}TM}{\partial n_{s}}$ with $\frac{\partial \lambda_{-}TM}{\partial n_{l}}$ which subsequently denoted as $\frac{\partial \lambda_{-}TE^{*}}{\partial n_{l}}$ and $\frac{\partial \lambda_{-}TM^{*}}{\partial n_{l}}$ including both effects of $n_s$ and $n_l$. The calculated thickness $a$ and refractive index $n_l$ via equation8 share the similar results compared with numerical values measured by DPI[25].

Given the values of biolayer thickness and refractive index, it is able to calculate the surface mass density during the binding event through De Feijter's formula[37]:$\rho_l$ =($n_l$ - $n_s$)/($dn$/$dc$), with $dn$/$dc$ the refractive index increment (in $cm^3$ $g^{-1}$) which in the case of protein and carbohydrate are 0.186 $cm^3$ $g^{-1}$ and 0.142 $cm^3$ $g^{-1}$ respectively. The density of adlayer dedicated by streptavidin, biotinylated heparin as well as HepV are 0.357g $cm^{-3}$, 0.322g $cm^{-3}$ and 0.336g $cm^{-3}$ respectively. Integrated with adlayer thickness and density, we can conclude that a thick sparse layer ($a$=5.46nm, $\rho_l$=0.322 g $cm^{-3}$) formed after heparin capture and a thin dense layer ($a$=5.33nm, $\rho_l$=0.336 g $cm^{-3}$) formed as HepV bound. This phenomenon can be explained that HepV undergoing conformational change on binding to heparin and a loss of streptavidin from waveguide surface during HepV injecting thereby a decrease of adlayer thickness and density, compared with streptavidin introduction.

## 2.6 DPHP waveguide fabrication

We have envisaged a CMOS-compatible fabrication process of the designed device. The process can start from a commercial SOI wafer. Alternatively the plasma enhanced chemical vapor deposition (PECVD) technology is used to deposit the $SiO_2$ and alpha-Si thin film on Si substrate. The photoresist thin film is formed on Si film and the waveguide patterns are constructed using an E-beam lithography so as to gain high resolution. Then an extreme thin



Brought to you by | University of Sussex Library
Authenticated
Download Date | 9/26/17 8:16 AM

aluminum (Al) film with 40nm thickness on the sidewall and 60nm thickness on the top of Si rib was deposited by sputtering process. This step could be followed by the deposition of a metal (Ag) layer with 3μm thickness on the sidewall and top of the Al film by sputtering process. Afterwards, Al film is removed by selectively etched to form the vertical and horizontal slots.

## 3. Conclusion

We have designed the dual polarization hybrid plasmonic(DPHP) waveguide and carried out a detailed investigation of modal properties and the performance of the proposed device. The employment of DPHP waveguide for protein analysis has been largely discussed. We take wavelength shift detection to quantify the molecular interaction with success. The relationship between biolayer property and resonance wavelength was deduced as equation8 in the text. The waveguide is capable of detecting shifts in biolayer thickness and refractive index without ambiguity, consequently distinguishing between a thick sparse layer and a thin dense layer. Associated with thickness and density of adlayer, we can catch sight to HepV undergoing conformational change when the binding event occurs. In addition, the propagation loss for the optimized size of waveguide can reach as low value as the order of $10^{-4}$. Last but not least, the novel device could be realized by a simple and CMOS-compatible fabrication process. In summary, the novel structure proposed with help of numerical and simulation analysis lays a good basis for the follow up work.

## Acknowledgement

The authors gratefully acknowledge the financial support for this work provided by the National Natural Science Foundation of China (NSFC) under Grant Nos. 61235003 and 61427816. This work was also supported by the Collaborative Innovation Center of Suzhou Nano Science and Technology.



Brought to you by | University of Sussex Library
Authenticated
Download Date | 9/26/17 8:16 AM

## References


[1] D. Nelson, and M. Cox. *Lehninger principles of biochemistry*. W.H. Freeman and Company, New York, 2005.

[2] SR Hammes. *The further redefining of steroid-mediated signaling. P NATL ACAD SCI USA* 2003,100,2168-2170.

[3] A Warshel, PK Sharma, M Kato, Y Xiang, HB Liu and Mats HM Olsson. *Electrostatic Basis for Enzyme Catalysis. Chem. Rev.* 2006, 106, 3210-3235.

[4] JA Roth, WK Hong, RU Komaki, AS Tsao, JY Chang and Shanda H. Blackmon. *Lung Cancer*. John Wiley & Sons, Inc., Hoboken, New Jersey , 2008.

[5] D. Barh A. Carpi, M. Verma and M. Gunduz. *Cancer Biomarkers: Minimal and Noninvasive Early Diagnosis and Prognosis*. Taylor and Francis, Boca Raton, FL, 2013.

[6] KE Coan, MJ Swann and J Ottl. *Measurement and Differentiation of Ligand-Induced Calmodulin Conformations Dual Polarization Interferometry. Anal. Chem.* 2012, 84, 1586-1591.

[7] F Dell'Olio, D Conteduca, C Cimineli and MN Armenise. *New ultrasensitive resonant photonic platform for label-free biosensing. Opt. Express* 2015, 23, 28593-28604.

[8] B. Drapp, J Piehler, A Brecht, G Gauglitz BJ Luff and J Ingenhoff. *Integrated optical Mach-Zehnder interfrometers as simazine imuunoprobes. Sens Act B.* 1997, 38–39, 277–282.

[9] B. Y. Shew, CH Kou, YC Huang and YH Tsai. *UV-LIGA interferometer biosensor based on the SU-8 optical waveguide. Sens. Act. A.* 2005,120, 383–389.

[10] F. Prieto, B Sepulveda, A Calle, A Llobera, C Dominguez, A Abad. A Montoya and LM Lechuga. *An integrated optical interferometric nanodevice based on silicon technology for biosensor applications. Nanotechnology* 2003, 14, 907–912.

[11] M Kitsara, K Misiakos, I Raptis and E Markarona. *Integrated optical frequency-resolved Mach-Zehnder interferometers for label-free affinity sensing. Opt. Express* 2010,18, 8193-8206.

[12] BJ Luff, James S. Wilkinson, J Piehler, U Hollenbach, J Ingenhoff and N Fabricius. *Integrated Optical Mach–Zehnder Biosensor. J LIGHTWAVE TECHNOL* 1998,16,583-592.

[13] WC Tsai and IC Li. *SPR-based immunosensor for determining staphylococcal enterotoxin A. Sens. Act. B*. 2009, 136, 8-12.

[14] Al Lao, X Su and KM Aung. *SPR study of DNA hybridization with DNA and PNA probes under stringent conditions. BIOSENS BIOELECTRON* 2009, 24,1717–1722.

[15] CT Yang, R Mejard, HJ Griesser, PO Bagnaninchi and B Thierry. *Cellular Micromotion Monitored by Long-Range Surface Plasmon Resonance with Optical Fluctuation Analysis. Anal. Chem.* 2015, 87,1456-61.

[16] *M Malmqvist. Biospecific interaction analysis using biosensor technology. Nature* 1993, 361, 186-187.




Brought to you by | University of Sussex Library
Authenticated
Download Date | 9/26/17 8:16 AM

[17] GH Cross, AA Reeves, S Brand, JF Popplewell, LL Peel, MJ Swann and NJ Freeman. *A new quantitative optical biosensor for protein characterization. BIOSENS BIOELECTRON* 2004, 19, 383-390.

[18] MJ Swann, LL Peel, S Carrington and NJ Freeman. *Dual-polarization interferometry: an analytical technique to measure changes in protein structure in real time, to determine the stoichiometry of binding events, and to differentiate between specific and nonspecific interactions. ANAL BIOCHEM* 2004, 329, 190-198.

[19] H Berney and K Oliver. *Dual polarization interferometry size and density characterisation of DNA immobilisation and hybridization. BIOSENS BIOELECTRON* 2005, 21, 618–626.

[20] MC Estevez, M Alvarez and ML Lechuga. *Integrated optical devices for lab-on-a-chip biosensing applications. LASER PHOTONICS REV* 2012, 6, 463-487.

[21] F Bahrami, MZ Alam, JS Aitchison and M Mojahedi. *Dual Polarization Measurements in the Hybrid Plasmonic Biosensors. Plasmonics* 2003, 8, 465-473.

[22] MZ Alam, F Bahrami, JS Aitchison and M Mojahedi. *Analysis and Optimization of Hybrid Plasmonic Waveguide as a Platform for Biosensing. IEEE PHOTONICS J* 2014, 6, 1-10.

[23] RJ Wenstrup, JB Florer, EW Brunskill, SM Bell, I Chervoneva and DE Birk. *Type V Collagen Controls the Initiation of Collagen Fibril Assembly. J BIOL CHEM* 2004, 279, 53331-53337.

[24] F Delacoux, A Fichard, C Geourjon, R Garrone and F Ruggiero. *Molecular Features of the Collagen V Heparin Binding Site. J BIOL CHEM* 1998, 273, 15069-15076.

[25] S Ricard-Blum, LL Peel, F Ruggiero and NJ Freeman. *Dual polarization interferometry characterization of carbohydrate–protein interactions. ANAL BIOCHEM* 2006, 352, 252-259.

[26] NM Green. Avidin. *Protein Chem.* 1975, 29, 85–133.

[27] David R. Lide, *CRC Handbook of Chemistry and Physics*, *Internet Version*, Taylor and Francis, Boca Raton, FL, 2007.

[28] CF Bohren and DR Huffman. *Absorption and Scattering of Light by Small Particle*. John Wiley &Sons, Inc., 1983.

[29] G Bartal, RF Oulton, VJ Sorger, X Zhang. *A Hybrid Plasmonic waveguide for Subwavelength Confinement and Long Range* ***Propagation****. NAT PHOTONICS* 2008,2,496-500.

[30] J Dostalek, J Ctyroky, J Homola, E Brynda, M Skalsky *et al. Surface plasmon resonance biosensor based on integrated optical waveguide. Sens Act B.* 2001,76,8-12

[31] H Awrin. *Ellipsometry on thin organic layers of biological interest: characterization and applications. Thin Solid Films* 2002, 377, 48-56

[32] J Wen and T Arakawa. *Refractive index of proteins in aqueous sodium chloride. ANAL BIOCHEM* 2000, 280, 327-329.

[33] TM Davis and WD Wilson. *Determination of the refractive index increments of small molecules for correction of surface plasmon resonance data. ANAL BIOCHEM* 2000, 284, 348-353.



Brought to you by | University of Sussex Library
Authenticated
Download Date | 9/26/17 8:16 AM

[34] GS Nikolic, MD Cakic and LA Ilic. *Specific refractive index increments of insulin. J. Serb. Chem. Soc.* 2001, 66, 397-401.

[35] M Kitsara, K Misiakos, I Raptis and E Makarona. *Integrated optical frequency-resolved Mach-Zehnder interferometers for label-free affinity sensing. Opt. Express* 2010, 18, 8193-8206.

[36] X Sun, D Dai, L Thylen and L Wosinski. *High-sensitivity liquid refractive-index sensor based on a Mach-Zehnder interferometer with a double-slot hybrid plasmonic waveguide. Opt. Express* 2015, 23, 25688-25699.

[37] JA De Feijter, J Benjamins and FA Veer. *Ellipsometry as a tool to study the adsorption behavior of synthetic and biopolymers at the air–water interface. Biopolymers* 1978,17,1759-1772.



Brought to you by | University of Sussex Library
Authenticated
Download Date | 9/26/17 8:16 AM

## Tables and figures

**Table 1** Observed layer characteristics[25] of thickness *a* and refractive index $n_l$ *during the whole process. Calculated solution refractive index* $n_s$ *in each step by equation* $n_l = 0.52*(n_p - n_s) + n_s$.

| Material (observation after each step) | Thickness *a* (nm) | RI of layer $n_l$ | RI of solution $n_s$ |
|---|---|---|---|
| Tris buffer | 0 | 0 | 1.366 |
| Streptavidin | 5.58 | 1.4037 | 1.3373 |
| Streptavidin + biotinylated heparin | 5.46 | 1.4077 | 1.3619 |
| HepV binding to heparin | 5.33 | 1.4073 | 1.3448 |

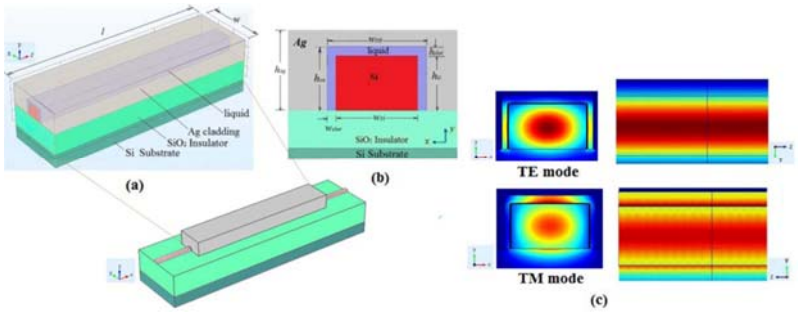


**Figure 1(a)** Schematic of DPHP waveguide. (b) Cross-section view of the DPHP waveguide filled by test liquid. The values of geometric parameters are $w_{slot}$ = 40nm, $h_{slot}$ = 60nm, $w_{si}$ = 550nm, $h_{si}$ = 320nm, $h_{Ag}$=3μm, $h_{sio2}$=3μm and $l$=25μm (c) Field profile of the DPHP waveguide.

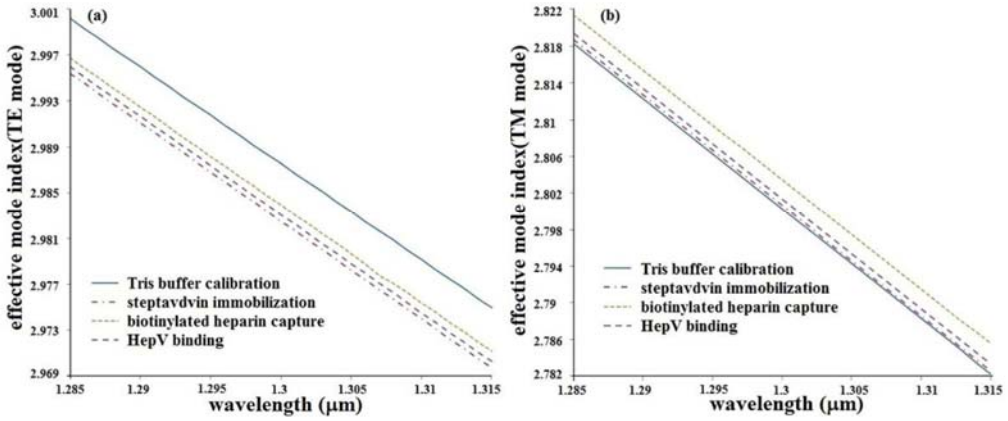


**Figure 2** Simulation results of HepV-heparin binding event at wavelength spanning 1.285μm ≤ $\lambda$ ≤ 1.315μm for TE mode (a) and TM mode (b) respectively. A plot of wavelength versus effective mode index provides a representation of each step.



Brought to you by | University of Sussex Library
Authenticated
Download Date | 9/26/17 8:16 AM

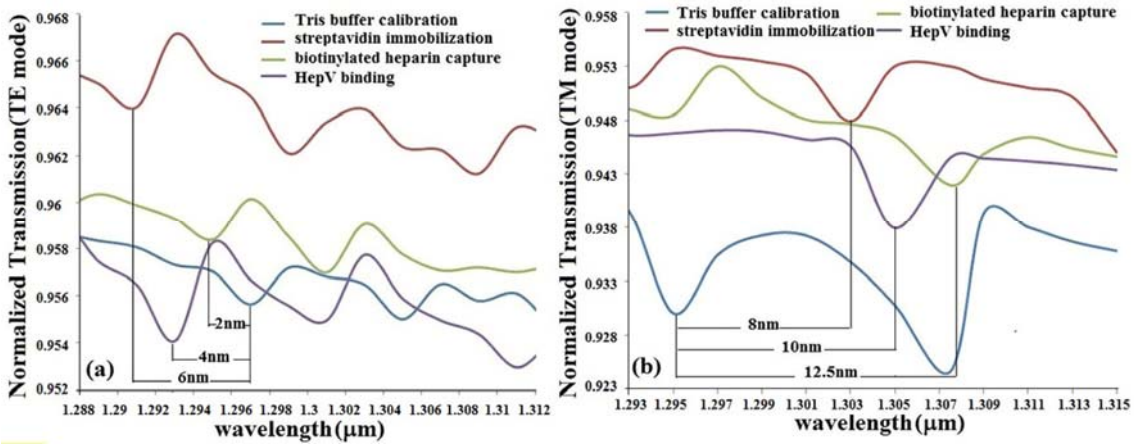


**Figure 3** The dependence of resonance wavelength on transmissions during the whole process for both TE mode (a) and TM mode (b).

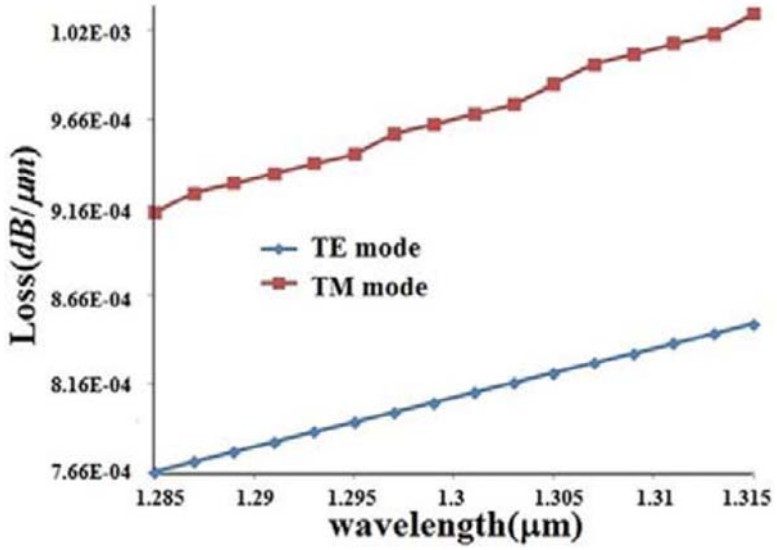


**Figure 4** Dependence of propagation loss on the wavelength varying from 1.285μm to 1.315μm for the optimized waveguide dimension for dual polarization. The value for loss can reach as low as the order of $10^{-4}$.



Brought to you by | University of Sussex Library
Authenticated
Download Date | 9/26/17 8:16 AM

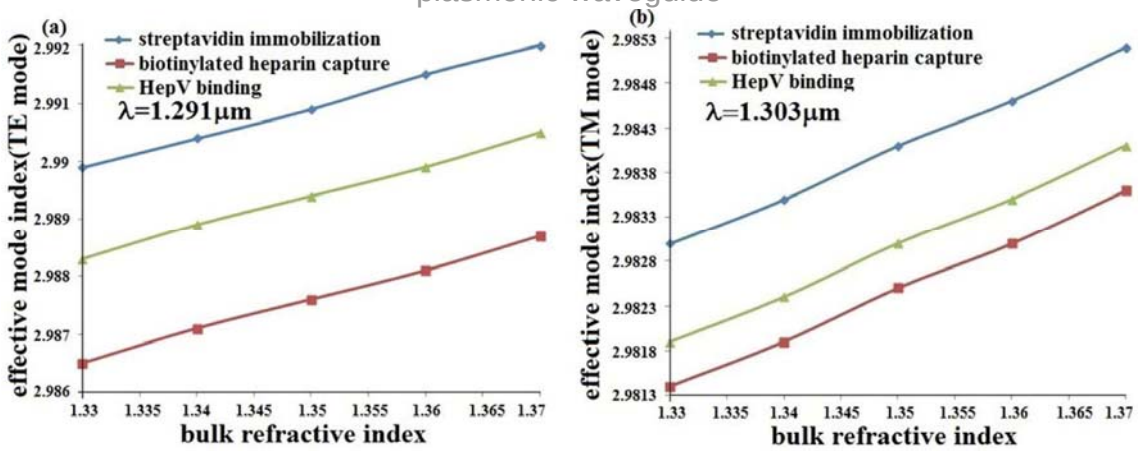


**Figure 5** The variation of transmission arising from different bulk refractive index($1.33 \leq n_s \leq 1.37$ with step 0.01) in the molecular binding event. (a) λ=1.291μm for TE mode, (b) λ =1.303μm for TM mode.

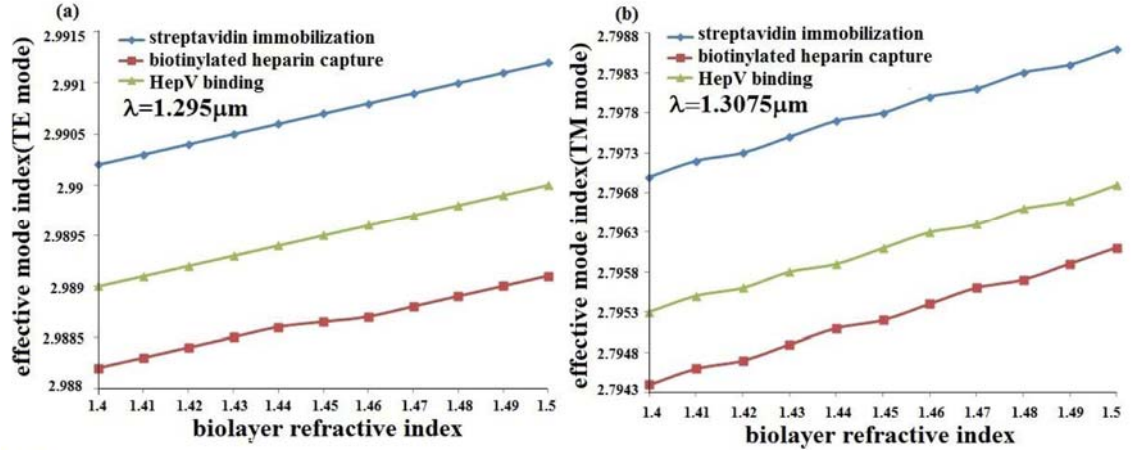


**Figure 6** The variation of transmission caused by biolayer index changing ($1.4 \leq n_l \leq 1.41$with step 0.01)during molecular interaction. (a) λ=1.295μm for TE mode, (b) λ =1.3075μm for TM mode.



Brought to you by | University of Sussex Library
Authenticated
Download Date | 9/26/17 8:16 AM

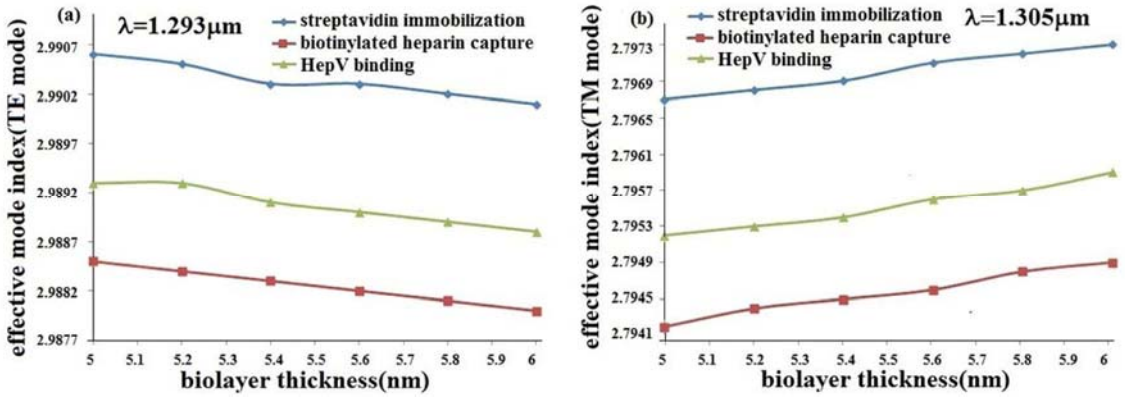


**Figure 7** The variation of transmission induced by the shift in adlayer thickness(5nm≤*a*≤6nm with step 0.2nm) during the molecular interaction. (a) λ=1.293μm for TE mode, (b) λ =1.305μm for TM mode.



Brought to you by | University of Sussex Library
Authenticated
Download Date | 9/26/17 8:16 AM